

# Probing the Core-Collapse Supernova Mechanism with Gravitational Waves

Christian D Ott

E-mail: [cott@tapir.caltech.edu](mailto:cott@tapir.caltech.edu)

Theoretical Astrophysics, Mailcode 350-17,  
California Institute of Technology, Pasadena, California 91125, USA

and  
Niels Bohr International Academy, Niels Bohr Institute,  
Copenhagen, Denmark

and  
Center for Computation and Technology, Louisiana State University,  
Baton Rouge, LA, USA

**Abstract.** The mechanism of core-collapse supernova explosions must draw on the energy provided by gravitational collapse and transfer the necessary fraction to the kinetic and internal energy of the ejecta. Despite many decades of concerted theoretical effort, the detailed mechanism of core-collapse supernova explosions is still unknown, but indications are strong that multi-D processes lie at its heart. This opens up the possibility of probing the supernova mechanism with gravitational waves, carrying direct dynamical information from the supernova engine deep inside a dying massive star. I present a concise overview of the physics and primary multi-D dynamics in neutrino-driven, magnetorotational, and acoustically-driven core-collapse supernova explosion scenarios. Discussing and contrasting estimates for the gravitational-wave emission characteristics of these mechanisms, I argue that their gravitational-wave signatures are clearly distinct and that the observation (or non-observation) of gravitational waves from a nearby core-collapse event could put strong constraints on the supernova mechanism.

PACS numbers: 97.60.Bw, 97.60.Jd, 97.60.-s, 97.10.Kc, 04.30.Db, 04.40.Dg

Submitted to the GWDW13 special issue of CQG on May 17, 2009.

## 1. Introduction

In their 1934 paper [1], Baade and Zwicky suggested that supernovae (SNe) are caused by the release of gravitational energy in the “collapse of ordinary stars to neutron stars.” Now, seventy-five years after this initial proposition and after much observational and theoretical effort, Baade’s and Zwicky’s statement still holds and is the fundamental paradigm of core-collapse SN theory.

Massive stars ( $\sim 8 - 10 M_{\odot} \lesssim M \lesssim 100 M_{\odot}$ ) live fast nuclear-burning lives, consuming their nuclear fuel in a cosmic blink of only  $\sim 100$  million – 1 million years ( $\tau/\tau_{\odot} \approx (M/M_{\odot})^{-2.5}$ ). When nuclear burning ceases in the core, a massive star has evolved to a red or blue supergiant (radius  $\sim \text{few} \times 10^{13}$  cm or  $\sim 0.1 - 1 \times 10^{12}$  cm, respectively) and is comprised of a central, compact Chandrasekhar-mass electron-degenerate iron core ( $R \sim 1500$  km) that is surrounded by an onion-skin structure of shells of material with successively lower mean atomic weight. Supported only

by increasingly relativistically-degenerate electrons, the iron core eventually exceeds its effective Chandrasekhar mass. Catastrophic gravitational collapse sets in and is accelerated by electron capture on nuclei and free protons as well as photodissociation of iron-group nuclei. In a matter of a few hundred milliseconds, the inner core is compressed from densities of  $10^9 - 10^{10} \text{ g cm}^{-3}$  to nuclear density ( $\sim 2.6 \times 10^{14} \text{ g cm}^{-3}$ ) where the nuclear equation of state (EOS) stiffens and stabilizes the inner core. The latter overshoots its new equilibrium, then rebounds into the still collapsing outer core. This *core bounce* results in the formation of a hydrodynamic shock at the interface of inner and outer core. The shock propagates outward in radius and mass through the supersonically infalling outer core material, leaving behind the unshocked  $\sim 0.5 - 0.7 M_\odot$  inner core which forms the core of the hot protoneutron star (PNS). The PNS rapidly gains mass through accretion ( $\dot{M}$  is of the order of  $1 M_\odot \text{ s}^{-1}$ ) and radiates away its gravitational energy ( $\sim 300 \text{ B}$  for a  $1.4 M_\odot$  NS;  $1 [\text{B}]_{\text{ethe}} = 10^{51} \text{ erg}$ ) in neutrinos as it evolves to a cold NS on a timescale of tens of seconds.

In early theory and SN models, a *prompt* hydrodynamic explosion would follow shock creation [2], removing the stellar envelope and providing the fantastic optical display of a SN with total kinetic, internal and electromagnetic energy of  $\sim 1 \text{ B}^\ddagger$ .

More advanced theory and simulations with more complete and accurate treatment of the EOS, neutrino physics and transport show that the prompt shock fails: Photodissociation of infalling heavy nuclei into nucleons (at a cost of  $\sim 8.8 \text{ MeV baryon}^{-1}$  for iron-group nuclei) and neutrinos that stream away from the optically-thin postshock region sap the shock's energy. The shock slows down quickly after its launch, stalls, and turns into an accretion shock at a radius of  $100 - 200 \text{ km}$ . For a SN explosion to occur, there must operate a *mechanism* that, in some fashion, transfers and deposits a fraction of the tremendous gravitational energy of collapse into the immediate postshock region, reviving the shock and endowing it with sufficient kinetic energy to make a core-collapse SN.

*What is the core-collapse SN mechanism?* This is the fundamental question and primary unsolved problem of core-collapse SN theory. Finding observational evidence for the SN mechanism by classical astronomical means from radio to  $\gamma$  wavelengths is difficult, since all pre-explosion dynamics takes place deep inside the stellar core, completely shrouded from view in the electromagnetic (EM) spectrum. Hence, EM observations yield only *secondary* observables, such as progenitor type and mass, explosion morphology and energy, ejecta composition, neutron star properties and birth kick. Primary, direct “live” information from deep inside the supernova engine is carried only by neutrinos and gravitational waves (GWs) which both can propagate from their emission sites to observers on Earth virtually without interaction with intervening matter.

GWs have not yet been observed directly, but an international network of interferometric detectors (LIGO, VIRGO, GEO, TAMA) is taking data with sufficient sensitivity to observe GWs from a nearby galactic core-collapse SN (e.g., [4, 5]). Neutrinos, on the other hand, were detected from SN 1987A, confirming the basic theory of stellar collapse and neutrino emission. However, in part due to the small number of detected neutrinos, this observation left unanswered the question of the SN mechanism.

In this contribution to the proceedings of the 13th Gravitational-Wave Data Analysis

$^\ddagger$  Inferred core-collapse SN energies fall in the range of  $0.1 - 10 \text{ B}$  [3], but energies around  $1 \text{ B}$  are most frequently seen.

Workshop (GWDAW13), I delineate the current set of proposed core-collapse SN mechanisms. I discuss the underlying physics of each mechanism and limit my focus to the dominant multi-D processes active and leading to GW emission in a given mechanism. Furthermore, I argue that the GW signatures of the various SN mechanisms are distinct and that the observation or non-observation of GWs by current and/or future advanced or third-generation GW observatories from a nearby SN can put significant constraints on the explosion mechanism. This idea was put forth first in [4] and is elaborated here. In section 2, I discuss the neutrino mechanism and its GW signature. This mechanism is currently favored as the explanation for core-collapse SN explosions in garden-variety slowly or nonrotating massive stars. Section 3 is devoted to the magnetorotational mechanism and its GW emission. This mechanism may be active in rapidly rotating massive stars. In section 4, I discuss the recently proposed acoustic mechanism of Burrows et al. [6, 7] which relies on the excitation of PNS pulsations and their damping via acoustic waves that steepen to shocks and efficiently deposit energy in the postshock region. In section 5, I summarize and draw conclusions.

## 2. The Neutrino Mechanism

The *neutrino-driven mechanism* (or simply, *neutrino mechanism*), is founded on the notion that if only a small fraction of the  $E_{\text{grav}} \sim 300 \text{ B}$  of gravitational energy liberated in collapse and emitted in neutrinos and antineutrinos of all flavors was deposited in the stellar mantle, it could be driven to explosion. The neutrino mechanism, based on the charged-current absorption of  $\nu_e$  and  $\bar{\nu}_e$  on neutrons and protons, respectively, was first proposed by Colgate & White [8] and Arnett [9] and was initially envisioned to be efficient and direct, that is, expected to drive the shock out before it has time to stall. However, simulations with improved numerics and input microphysics showed that neutrino energy deposition (“neutrino heating”) is actually rather inefficient and the shock always stalls first and may be revived only on a timescale of hundreds of milliseconds in the *delayed neutrino mechanism* proposed by Bethe & Wilson [10]. The amount of energy to be delivered by the mechanism,  $E_{\text{mech}}$ , is set by the sum of asymptotic explosion energy of  $\sim 1 \text{ B}$  and the gravitational binding energy of the mantle (also of the order of 1 B) that must first be overcome. Hence,  $E_{\text{mech}}/E_{\text{grav}} \sim 1\%$  is the fraction of the total energy that must be transferred to the mantle by neutrinos to power an explosion. This 1% must be provided to the shock within a short,  $\lesssim 1 - 2 \text{ s}$  time frame after bounce in order for the onset of explosion to occur before accretion has pushed the PNS over its maximum mass and for the SN to leave behind a NS mass consistent with observations. Typical  $\nu_e$  and  $\bar{\nu}_e$  luminosities in the postbounce phase are  $L_{\nu_e} \approx L_{\bar{\nu}_e} \approx 10 \text{ B s}^{-1}$  and, hence, assuming that the explosion must start within  $\sim 1 \text{ s}$ , the necessary *heating efficiency* is of the order of  $\sim 10\%$ .

As compelling and promising the neutrino mechanism may seem, the most advanced simulations predict its failure in ordinary massive stars with masses  $\gtrsim 10 M_{\odot}$  when spherical symmetry (1D) is assumed and fluid motions are restricted to the radial direction [11, 12, 13]. Only the lowest-mass massive stars with  $7 M_{\odot} \lesssim M \lesssim 10 M_{\odot}$  (S-AGB stars that end their nuclear burning lives with O-Ne cores) may explode, though sub-energetically, by the 1D neutrino mechanism alone [14, 15]. In multi-D, neutrino-driven convection [16, 17, 18] in combination with the standing-accretion-shock

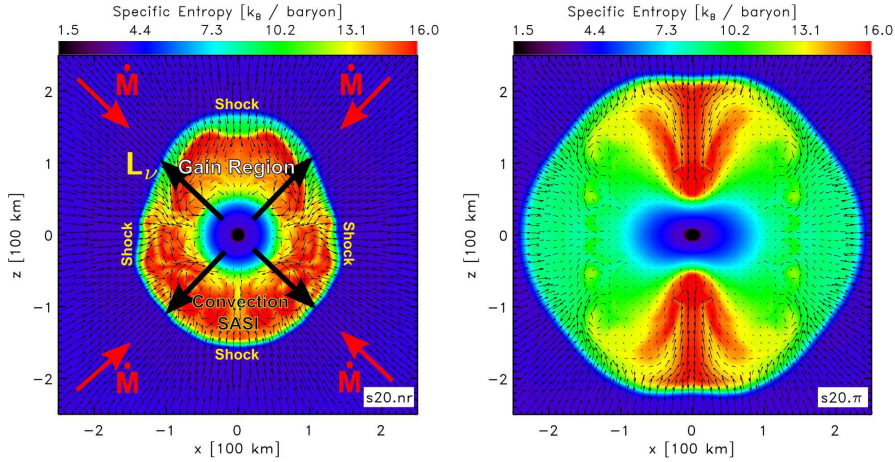


**Figure 1.** Postbounce supernova cores of the nonrotating model s20.nr (left panel) and the rapidly-spinning model s20.π (right panel) of the angle-dependent neutrino-radiation-hydrodynamics simulations of Ott et al. [25] at  $\sim 215$  ms after bounce. Shown are the specific entropy distributions and velocity vectors are superposed to visualize flow patterns. Key aspects of the postbounce situation are highlighted in model s20.nr in the left panel.

instability (SASI) (e.g., [19, 20, 21] and references therein) can enhance the heating efficiency [22, 23]. Yet, the presently most complete axisymmetric (2D) simulations still fall short of producing robust 1-B neutrino-driven explosions [6, 22, 24, 25] and hope for the neutrino mechanisms rests on the additional degrees of freedom provided by 3D dynamics to facilitate robust explosions in nature and in future detailed 3D simulations [20, 23, 26].

Figure 1 displays color maps of the specific entropy distribution in snapshots taken at  $\sim 215$  ms after bounce of the simulations of Ott et al. [25] that started with a  $20-M_{\odot}$  presupernova model and were carried out without rotation (model s20.nr) and with rapid precollapse rotation (model s20.π,  $\Omega_0 = \pi \text{ rad s}^{-1}$ ). Simulation details are explained at length in [25]. The nonrotating model is depicted in the left panel and the various features of the postbounce situation are highlighted by text and arrows. Neutrinos are trapped in the dense PNS core, but leak out from the neutrinosphere $\S$  at the PNS surface. Neutrino cooling ( $Q_{\nu}^{-} \propto T^6$ , e.g., [27]) dominates over neutrino heating ( $Q_{\nu}^{+} \propto L_{\nu} r^{-2} \langle \epsilon_{\nu}^2 \rangle$ , [27]) interior to the gain radius of 80 – 100 km denoting the location beyond which  $Q_{\nu}^{+} > Q_{\nu}^{-}$ . The net neutrino heating is strongest near the inner boundary of the gain region and decreases outwards. Hence, a negative entropy gradient develops, resulting in instability to overturn and convective eddies in the gain region are clearly visible. Also discernible is the deformation of the shock front due to the early phase of the SASI which drives the growth of low-mode ( $\ell = 1, 2$ ) perturbations in an advective-acoustic cycle of laterally propagating sound waves and advection of pressure perturbations (e.g., [21] and references therein).

$\S$  The neutrinosphere is defined as the location at which the neutrino optical depth  $\tau_{\nu}$  is  $2/3$ . The radius  $R_{\nu}$  of the neutrino sphere is strongly dependent on neutrino energy.

### 2.1. Convection and SASI in Nonrotating and Rotating SN Cores

In the core-collapse SN context, convective instability can generally be driven by negative gradients in entropy  $s$  or lepton fraction  $Y_l = Y_e + Y_\nu$ . Rotation or more specifically, a positive specific angular momentum gradient, can stabilize the flow against overturn. This is expressed in the Solberg-Høiland condition for instability. In the equatorial plane and neglecting lateral gradients, this condition is given by

$$N^2 + \frac{1}{r^3} \frac{d}{dr} j^2 < 0. \quad (1)$$

Here,  $j = \Omega r^2$  is the specific angular momentum and  $N^2$  is the Brunt-Väisälä frequency, in the SN context [28, 29],

$$N^2 = \frac{g}{p\gamma} \left( \left. \frac{\partial p}{\partial s} \right|_{\rho, Y_l} \frac{ds}{dr} + \left. \frac{\partial p}{\partial Y_l} \right|_{\rho, s} \frac{dY_l}{dr} \right), \quad (2)$$

where  $g$  is the gravitational acceleration,  $\gamma = d \ln p / d \ln \rho|_s$ , and  $\partial p / \partial s$  and  $\partial p / \partial Y_l$  are generally positive. In the right panel of figure 1, the entropy distribution and the superposed velocity vector field of the rapidly spinning (PNS period  $\sim 2$  ms) oblate postbounce SN core of model s20. $\pi$  is shown at  $\sim 215$  ms after bounce. The large positive specific angular momentum gradient in its equatorial regions makes the left-hand side of eq. (1) positive and convective overturn is confined to regions near the axis and large equatorial radii where the  $j$ -gradient flattens off. The shock in model s20. $\pi$  is deformed to oblate shape and its average radius is considerably greater than at the same time in the nonrotating model, but a top-bottom asymmetry typical for the SASI is absent. According to the results of Ott et al. [25], rotation not only inhibits convection, but also delays and alters the growth of the axisymmetric SASI significantly. As pointed out by [30, 31], the situation may be different in 3D where a spiral-type azimuthal SASI may develop in rapidly rotating SN cores.

In nonrotating and slowly rotating core-collapse SNe, convection generically occurs in three distinct ways: (1) Prompt convection, driven by the negative entropy gradient left behind by the stalled shock and strongly dependent on the seed perturbations present in the core [4, 24], (2) as lepton-gradient driven convection in the PNS (e.g., [22, 32, 33]), and (3) as the already mentioned neutrino-driven convection in the gain region behind the shock (e.g., [6, 16, 17, 18, 22]).

### 2.2. GW Emission

In nonrotating or slowly rotating core-collapse SNe and in the absence of strong PNS pulsations (discussed in section 4), the dominant multi-D dynamics and, hence, the primary emission process of GWs is associated with convective overturn and the SASI. In addition, and also related to the asymmetry due to convection and SASI, anisotropic emission of neutrinos adds a slowly-varying component to the GW signal with characteristic frequencies of the order of 10 Hz. Recent quantitative estimates of the latter can be found in [4, 34, 35]. Here, I focus on the higher-frequency, more readily-detectable GW signal from fluid motions and present in the left-hand panel of figure 2 the GW signal from the postbounce simulations of Ott et al. [25] (models s20.nr and s20. $\pi$  as discussed above) that were run with full 2D angle-dependent neutrino-radiation hydrodynamics. The GW signals include the contributions from PNS convection, neutrino-driven convection and SASI. Scaled to a fiducial galactic

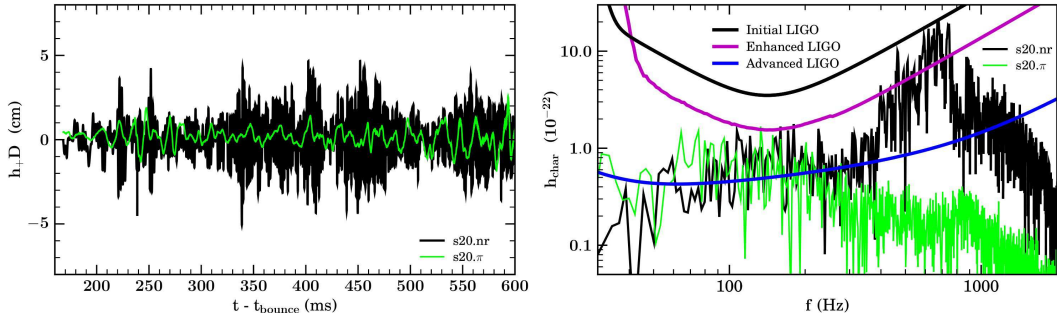


**Figure 2.** **Left:** GW signal  $h_+$  (scaled by the source distance  $D$  and in units of cm) of convection in the PNS and neutrino-driven convection and SASI in the postshock region in the axisymmetric postbounce models s20.nr (nonrotating, black lines) and s20. $\pi$  (rapidly rotating, green lines) of [25]. Rapid rotation effectively damps convection and modifies the SASI, leading to a lower-amplitude and more slowly varying GW signal. **Right:** Characteristic strain spectra  $h_{\text{char}}$  [36] of the same GW signals assumed to be emitted at  $D = 10$  kpc and contrasted with theoretical initial, enhanced, and advanced LIGO design noise curves. Note that, in practice, initial LIGO’s low-frequency sensitivity is identical to that of enhanced LIGO [37].

source distance of 10 kpc, the peak amplitudes correspond to a dimensionless GW strains of  $\sim 1.3 \times 10^{-22}$  and are reached by the nonrotating model s20.nr. Convection in the rapidly rotating model is strongly inhibited, both in the PNS and in the postshock region. This is reflected in its low-amplitude, slowly-varying GW signal.

In the right panel of figure 2, I plot the characteristic gravitational wave strain of the two postbounce SN models, defined by Flanagan & Hughes [36] as  $h_{\text{char}}(f) = D^{-1} \sqrt{2\pi^{-2} G c^{-3} dE_{\text{GW}}/df^{-1}}$ , where  $D$  is the distance to the source (set to 10 kpc) and  $dE_{\text{GW}}/df$  is the GW spectral energy density. In order to contrast the  $h_{\text{char}}$  spectra with detector sensitivity, I also plot the design sensitivity  $h_{\text{rms}}$  of initial LIGO [38], enhanced LIGO [39], and advanced LIGO (in burst mode) [40]. According to the simulation data of Ott et al., in a nonrotating or slowly-rotating SN, most of the energy in GWs is emitted in a broad frequency range of 300 – 1000 Hz (this is in rough agreement with [24]) by a combination of the high- $f$ , small-scale PNS convection and downflow plumes of material caused by the SASI that penetrate to small radii and are rapidly decelerated at the PNS surface [4, 24]. The emission due to convection in the rapidly rotating model is much weaker, lacks the high- $f$  component and occurs primarily at frequencies of  $\sim 10 - 200$  Hz.

It is important to note two aspects: (1) The nature of the GW emission by convection and SASI is stochastic [4, 35] and the emitted GWs will be of uncorrelated, essentially random polarization. This is a consequence of the turbulent, chaotic emission dynamics that depend in a non-deterministic fashion on local conditions and can vary greatly from one SN to the next. (2) The detectability of the GWs from convection and SASI (i.e., the magnitude of  $h_{\text{char}}$  in the right panel of figure 2) depends crucially on the duration of emission. The SASI and neutrino-driven convection shut off once an explosion has fully developed or a BH has formed. Hence, it may last  $\sim 200$  ms – 3 s, the upper limit depending on the onset of explosion, the accretion rate set by the progenitor and the EOS-dependent mass-limit for BH formation. PNS convection would be shut off by BH formation, but if an energetic explosion occurs,

it is likely to continue for many seconds until the PNS has reached neutrino-less  $\beta$ -equilibrium. See [4] for scalings of the emitted GW energy with the duration of the convective signal.

### 3. The Magnetorotational Mechanism

Most ( $\gtrsim 99\%$ ) core-collapse SN progenitors are expected to be rather slowly rotating and have central periods of tens to hundreds of seconds [41, 42]. However, there exists a variety of progenitor channels that could yield iron cores with precollapse periods of the order of seconds (e.g., [43, 44]). Conservation of angular momentum in collapse leads to a spin-up by a factor of  $\sim 1000$  [42]. Hence, an iron core with  $P_0 \sim 2$  s results in a PNS with  $P \sim 2$  ms and a rotational energy of the rigidly-rotating PNS and of the strongly differentially rotating postshock layer of a few  $\times 10$  B [42, 45]. A fraction of this energy would be sufficient to power an energetic core-collapse SN provided there is an efficient mediating mechanism for converting rotational energy into linear kinetic energy of the ejecta.

Theory and early simulations [46, 47, 48, 49] have shown that magnetorotational processes may constitute such a mechanism and can drive collimated outflows, leading to energetic jet-driven bipolar explosions [50]. Recently, this *magnetorotational* mechanism has received much attention (e.g., [45, 51, 52, 53, 54] and references therein) owing to increasing observational evidence for collimated jets in the context of gamma-ray bursts (GRBs) and hypernovae (hyper-energetic  $\gtrsim 10$ -B SNe) and the association of stellar collapse with the long-soft class of GRBs (e.g., [55]).

Recent simulations [45, 52, 53, 54, 56] suggest that magnetic fields of the order of  $10^{15}$  G with strong toroidal components are required to yield the necessary magnetic stresses to drive a strong bipolar explosion. Rapidly rotating progenitors may have rather strongly magnetized cores, with toroidal fields of  $\sim 10^9 - 10^{11}$  G (the poloidal components are 1 – 2 orders of magnitude weaker) [41, 43]. Flux compression in collapse scales  $\propto (\rho/\rho_0)^{2/3}$  [45, 52] and can lead to an amplification of both toroidal and poloidal components by up to a factor of 1000. Further amplification is provided for the toroidal component by rotational winding of poloidal into toroidal field ( $\Omega$ -dynamo, e.g., [45, 52, 57], a linear process) and by the exponentially-growing magnetorotational instability (MRI, e.g., [45, 51, 52, 58] and references therein) that has the potential to provide dynamically-relevant saturation field strengths of the order of  $10^{15}$  G [58]. Both,  $\Omega$ -dynamo and MRI operate on rotational shear ( $d\Omega/d\ln r$ ) and convert energy stored in differential rotation<sup>||</sup> into magnetic field. Strong differential rotation in the outer SN core is a generic feature of rotating core collapse [42, 59].

The to-date most microphysically complete MHD core-collapse simulations (though in a Newtonian framework) were carried out by Burrows and collaborators [45, 56]. Under the provision that the MRI operates as expected [58] and the postbounce rotational energy is of the order of  $\sim 10$  B (implying  $P_0 \lesssim 4$  s), these authors find robust and powerful bipolar magnetorotational explosions that reach hypernova energies, leave behind a protomagnetar and could be the stage-setting precursor to a subsequent GRB [45, 56].

<sup>||</sup> The lowest-energy state of a rotating fluid at fixed total angular momentum is uniform rotation. Hence, the difference in energy between uniform and differential rotation at fixed total angular momentum can be considered as “free energy of differential rotation.”

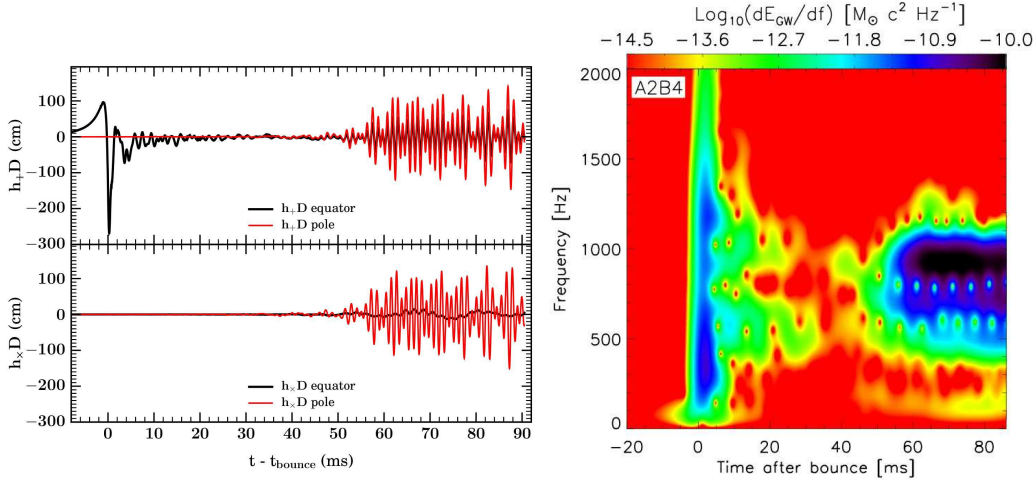


**Figure 3.** **Left:** GW signal (rescaled by distance  $D$  and in units of cm) emitted by rotating core collapse, bounce and postbounce nonaxisymmetric dynamics in model s20A2B4 of [60, 61]. Shown are the  $h_+$  (top) and  $h_\times$  (bottom) polarizations as seen by observers situated in the equatorial plane (red lines) and along the polar axis (black lines). Note that the GWs are linearly polarized during the axisymmetric collapse and bounce phase and become predominantly elliptically polarized only tens of milliseconds after bounce. This panel is a variant of the right panel of figure 4 in [4]. **Right:** Time-frequency (TF) analysis of the spectral energy density of the GWs emitted by model s20A2B4. The TF analysis was carried out with a 2-ms Gaussian window that was shifted over the data in steps of 0.2 ms. Both the strong burst at core bounce and the energetic late postbounce emission leave clear and clearly separated marks in the TF diagram.

### 3.1. GW Emission

Without any reasonable doubt one can assume that rapid rotation is the primary multi-D component of the magnetorotational mechanism. Rapid rotation leads to a strong burst of GWs at core bounce, associated with the huge accelerations acting on the centrifugally deformed inner core. This GW emission process is the most extensively studied in the core-collapse context (see, e.g., [4] for a review) and the currently best estimates of the GW signal come from 2D and 3D GR simulations that include a microphysical EOS and deleptonization during collapse [60, 61, 62, 63]. These studies have demonstrated that the GW signal from bounce is of generic morphology, exhibiting a small pre-bounce rise, a large negative peak roughly coincident with bounce and a subsequent ringdown signal emitted as the PNS settles to its new quasi-hydrostatic configuration. Comparing 2D and 3D simulations, [60, 61] demonstrated that even extremely rapidly rotating cores stay axisymmetric through bounce, which constrains the GW emission to linear polarization (emission only in  $h_+$ ). According to the results of [63], a core collapsing with a precollapse period  $P_0 \sim 2$  s ( $P_0 \sim 4$  s) located at 10 kpc emits a peak GW amplitude of  $|h_{\max}| \sim 1 \times 10^{-21}$  ( $|h_{\max}| \sim 5 \times 10^{-21}$ ) and a total energy in GWs of the order of a few  $\times 10^{-8} M_\odot c^2$  with most of the emission being concentrated at 500 – 800 Hz, extending to lower frequencies with increasing rotation.

Although realistic PNSs are unlikely to undergo the classical dynamical MacLaurin-type nonaxisymmetric instability at rotation rates  $T/|W| \gtrsim 27\%$  [63], nonaxisym-



metric dynamics may still develop via a low- $T/|W|$  corotation instability [64]. For equilibrium NS models, this was first discovered by [65] and has since been found to occur also in more realistic postbounce SN settings [60, 61, 66, 67].

In the left panel of figure 3, I plot the gravitational wave polarizations  $h_+$  (top) and  $h_\times$  (bottom) as seen by equatorial (black lines) and polar observers (red lines) emitted by model s20A2B4 in the 3 + 1 GR framework of Ott et al. [60, 61]. This model used a  $20-M_\odot$  progenitor with an iron core set up to spin roughly uniformly at a period of  $\sim 1$  s. The purely axisymmetric ( $\ell = 2, m = 0$  in terms of spherical harmonics) bounce signal is followed by a primarily axisymmetric ringdown. Nonaxisymmetric dynamics develops in the postbounce phase and becomes relevant some 40 ms after bounce as indicated by the rise of the GW signal emitted along the poles ( $\ell = 2, m = 2$ ) due to the quadrupole components of the nonaxisymmetric dynamics. The right panel of the same figure displays a time-frequency analysis of the GW spectral energy density. The quick change in the waveform at bounce leads to power in a broad range of frequencies, but most of the energy is emitted around 350–400 Hz in this rather rapidly rotating core. The nonaxisymmetric component kicks in at higher frequencies around  $\sim 900 - 950$  Hz (with secondary, modulating components at  $\sim 700$  Hz and  $\sim 500$  Hz) and, despite emitting lower-amplitude GWs, is significantly more energetic than the bounce signal, emitting roughly  $E_{\text{GW}} \sim 1.6 \times 10^{-7} M_\odot c^2$  until the simulation was terminated. The nonaxisymmetric dynamics could last longer, possibly for hundreds of milliseconds [4, 61], but may be in competition with the MRI, an aspect that remains yet to be investigated.

#### 4. The Acoustic Mechanism

The *acoustic mechanism*, proposed in a series of papers by Burrows and collaborators [6, 7, 68] (using 2D radiation-hydrodynamic simulations), is based on the excitation of PNS core pulsations (primarily  $\ell = \{1, 2\}$   $g$ -modes) by turbulence and by accretion downstreams through the unstable and highly-deformed stalled shock in the non-linear phase of the SASI. In the simulations of Burrows et al., fueled by the gravitational energy of anisotropic accretion, the PNS pulsations ramp up to non-linear amplitudes over many hundreds of milliseconds and damp via the emission of strong sound waves. These travel down the steep density gradient present in the postshock region, thus steepen to shocks and very efficiently deposit their energy behind and in the shock. Explosions in the acoustic mechanism are robust, but set in only after  $\sim 1$  s after bounce and tend to have energies on the lower side of what is observed.

There are multiple caveats associated with the acoustic mechanism: (1) It is so far unconfirmed, but also not yet ruled out by other SN groups (e.g., [24]). (2) Perturbation theory suggests that the PNS mode amplitudes may be limited by a parametric instability involving high-order modes that are not presently resolved in numerical simulations [69]. (3) If the neutrino mechanism is effective, it will probably explode the star before the PNS pulsations have time to grow to large amplitudes. (4) As pointed out in section 2, rapid rotation has a stabilizing effect on convection and SASI and, hence, is likely to also inhibit the growth of PNS pulsations. In addition, rapidly rotating SNe are likely to explode by the magnetorotational mechanism much before PNS pulsations can reach large amplitudes. (5) It is not clear how the relaxation of axisymmetry would affect the power and spatial character of the PNS pulsations. 3D simulations have yet to be performed.

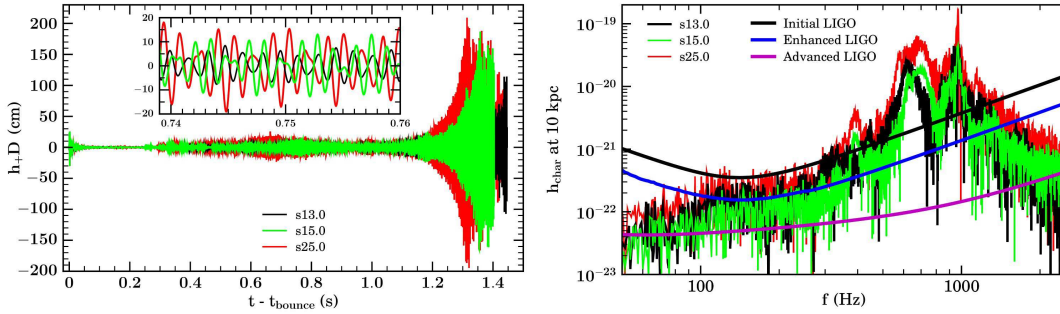


**Figure 4.** **Left:** GW signals (rescaled by distance  $D$  and in units of cm) emitted in a set of representative nonrotating models from [7] that explode via the acoustic mechanism. At early times, the GW signal contains a burst associated with prompt convection at bounce and a longer-term broad-band low-amplitude contribution from PNS convection, neutrino-driven convection, and the SASI. At later times ( $t \gtrsim 300 - 600$  ms after bounce), the GW emission becomes dominated by PNS core pulsations, leading to a narrowband signal (a zoomed-in view is shown in the inset plot). Around the time of the onset of explosion the largest GW amplitudes are reached. **Right:** Characteristic GW strain spectra  $h_{\text{char}}$  [36] (at 10 kpc) of the same models contrasted with initial, enhanced and advanced LIGO design noise curves.

#### 4.1. GW Emission

The early postbounce GW emission associated with the acoustic mechanism is similar to that of the neutrino mechanism discussed in section 2.2 and comes primarily from convection, the SASI and SASI downflow plumes that are decelerated at the PNS core’s outer edge. The latter are drivers of the PNS pulsations whose quadrupole components dominate the GW emission in the later postbounce phase. They are the most characteristic dynamical feature of the acoustic mechanism.

In the left panel of figure 4, I plot sample GW signals extracted from the simulations of Burrows et al. [7] (a more detailed discussion of these models was presented in [4]) for a variety of progenitors. Present is a burst of prompt convection around core bounce, followed by a phase of neutrino-driven convection with little SASI. Around  $\sim 300 - 600$  ms after bounce, the non-linear SASI regime is reached, downflow plumes reach the PNS core and the core pulsations begin to grow and emit GWs at the frequencies of their quadrupole components (see inset plot) that are set by the core’s structure. While the GW emission in these models at intermediate times stems from  $\ell = 2$  harmonics of the then dominant  $\ell = 1$  mode, an  $\ell = 2$  eigenmode at higher frequencies appears dominant at times  $\gtrsim 1 - 1.2$  s, explaining the increase of the GW amplitudes around the onset of explosion.

The PNS core pulsations of the acoustic mechanism are the strongest GW emission mechanism proposed in the stellar collapse context. Predicted strain amplitudes range up to  $h_+ \sim 10^{-20}$  (at 10 kpc, [4]) and total GW energies are  $E_{\text{GW}} \sim 10^{-7} M_{\odot} c^2$  and above, emitted in a narrow frequency band set by the PNS pulsation frequencies and their temporal evolutions. The right panel of figure 4, contrasting  $h_{\text{char}}$  spectra with detector design sensitivities, demonstrates that a galactic SN exploding via the acoustic mechanism would be difficult to miss even with first-generation detectors.

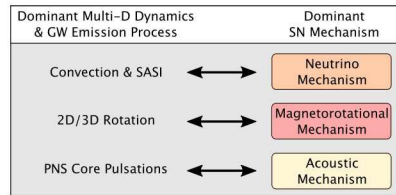


**Figure 5.** Scheme summarizing the associations of particular multi-D processes and characteristic GW emissions with the individual candidate core-collapse SN mechanisms.

## 5. Discussion and Conclusions

Each of the three SN mechanism that I consider in this article has an unique multi-D dynamical process intimately linked with it. The acoustic mechanism, while involving neutrino-driven convection and SASI, is fundamentally reliant on non-linear PNS core pulsations to drive the acoustic SN engine. In the magnetorotational mechanism, on the other hand, rapid rotation is the key ingredient, damping convection and SASI, and facilitating B-field amplification and a bipolar jet-driven explosion. Finally, the neutrino mechanism’s key multi-D aspect is convection and SASI. While PNS core pulsations could certainly be excited, they would not have time to grow to large amplitudes if the neutrino mechanism was effective and launched an early explosion.

Now, as delineated in the previous sections and portrayed by figures 2–4, the three distinct multi-D processes dominant in the three SN mechanisms have very different GW emission characteristics: (1) Convection and SASI of the neutrino mechanism lead to a low-amplitude, broadband “stochastic” signal. (2) The rapid rotation necessary for the magnetorotational mechanism is reflected in GWs by a strong axisymmetric burst at core bounce and a possible prolonged narrowband postbounce GW signal from nonaxisymmetric dynamics. (3) The strong PNS core pulsations of the acoustic mechanism – if they obtain – emit copiously in narrow intervals about their characteristic frequencies.

With the above information a simple picture can be drawn (figure 5), relating a particular SN mechanism with a particular flavor of multi-D dynamics and an unique GW signature. Hence, with an observation of GWs from a core-collapse SN, the first strong observational constraints could be put on the SN mechanism. The magnetorotational and acoustic mechanisms should be clearly visible throughout the Milky Way with initial and enhanced interferometric detector technology while advanced and probably third-generation observatories (e.g., ET [70]) may be needed to constrain the SN mechanism for core-collapse events at 3 – 5 Mpc out to which the integrated SN rate is  $\sim 0.5 \text{ yr}^{-1}$  [4, 71]. Due to the low-amplitude, broadband nature of its GW emission, the neutrino mechanism is the most difficult to detect in GWs, but a non-detection of GWs from a galactic event with initial and enhanced detectors would quite clearly rule out the other two candidate mechanisms.

The way in which I have portrayed the candidate SN mechanisms and their GW signatures in this article is idealized: I have focussed only on the primary multi-D dynamics in each mechanism and its associated GW emission, neglecting contributions from secondary and, in particular, low-frequency components, such as GWs from anisotropic neutrino emission, magnetic stresses, or explosion asymmetries (see [4] for

a detailed discussion). I have also neglected the possibility of the combined action of multiple mechanisms. For example, an explosion could be driven by a combination of neutrino heating and MHD processes in a moderately rapidly rotating SN. Yet, even in such a case, the dominant dynamical multi-D component would also dominate the GW emission and the simple scheme displayed in figure 5 is essentially preserved.

Further theoretical and physically more complete and accurate computational work is necessary to gain a better understanding of the various possible SN mechanisms and of the details of their GW signatures. But, as I have attempted to show in this article, even with current knowledge, the GW signal of a galactic SN today may very likely provide strong hints for one mechanism and/or smoking-gun evidence against another.

### Acknowledgements

It is a pleasure to thank E. O'Connor, E. Abdikamalov, R. Adhikari, A. Burrows, L. Cadonati, L. Dessart, H. Dimmelmeier, I. S. Heng, H.-T. Janka, E. Katsavounidis, S. Klimentenko, K. Kotake, A. Marek, C. Meakin, J. Murphy, R. O'Shaughnessy, B. Owen, C. Pethick, E. S. Phinney, E. Schnetter, U. Sperhake, and K. Thorne for helpful and stimulating discussions. This work was supported by a Sherman Fairchild postdoctoral fellowship at Caltech and by an Otto Hahn Prize awarded to the author by the Max Planck Society. Results presented in this article were obtained through computations on the NSF Teragrid under grant TG-MCA02N014, on machines of the Louisiana Optical Network Initiative under grant LONI\_NUMREL03, and at the National Energy Research Scientific Computing Center (NERSC), which is supported by the Office of Science of the US Department of Energy under contract DE-AC03-76SF00098.

### References

- [1] W. Baade and F. Zwicky. *Proc. Nat. Acad. Sci.*, **20**, 259, 1934.
- [2] H. A. Bethe. *Rev. Mod. Phys.*, **62**, 801, 1990.
- [3] M. Hamuy. *Astrophys. J.*, **582**, 905, 2003.
- [4] C. D Ott. *Classical and Quantum Gravity*, **26(6)**, 063001, 2009.
- [5] Abbot, B. P. et al., Ligo Scientific Collaboration. *arXiv:0905.0020 [gr-qc]*, 2009.
- [6] A. Burrows, E. Livne, L. Dessart, C. D. Ott, and J. Murphy. *Astrophys. J.*, **640**, 878, 2006.
- [7] A. Burrows, E. Livne, L. Dessart, C. D. Ott, and J. Murphy. *Astrophys. J.*, **655**, 416, 2007.
- [8] S. A. Colgate and R. H. White. *Astrophys. J.*, **143**, 626, 1966.
- [9] W. D. Arnett. *Canadian Journal of Physics*, **44**, 2553, 1966.
- [10] H. A. Bethe and J. R. Wilson. *Astrophys. J.*, **295**, 14, 1985.
- [11] M. Rampp and H.-T. Janka. *Astrophys. J. Lett.*, **539**, L33, 2000.
- [12] T. A. Thompson, A. Burrows, and P. A. Pinto. *Astrophys. J.*, **592**, 434, 2003.
- [13] M. Liebendörfer, M. Rampp, H.-T. Janka, and A. Mezzacappa. *Astrophys. J.*, **620**, 840, 2005.
- [14] F. S. Kitaura, H.-T. Janka, and W. Hillebrandt. *Astron. Astrophys.*, **450**, 345, 2006.
- [15] A. Burrows, L. Dessart, and E. Livne. The Multi-Dimensional Character and Mechanisms of Core-Collapse Supernovae. In S. Immler and R. McCray, editors, *AIP Conference Series*, volume 937, page 370, 2007.
- [16] M. Herant, W. Benz, W. R. Hix, C. L. Fryer, and S. A. Colgate. *Astrophys. J.*, **435**, 339, 1994.
- [17] A. Burrows, J. Hayes, and B. A. Fryxell. *Astrophys. J.*, **450**, 830, 1995.
- [18] H.-T. Janka and E. Müller. *Astron. Astrophys.*, **306**, 167, 1996.
- [19] L. Scheck, H.-T. Janka, T. Foglizzo, and K. Kifonidis. *Astron. Astrophys.*, **477**, 931, 2008.
- [20] W. Iwakami, K. Kotake, N. Ohnishi, S. Yamada, and K. Sawada. *Astrophys. J.*, **678**, 1207, 2008.
- [21] R. Fernández and C. Thompson. *submitted to ApJ, arXiv:0812.4574*, 2008.

- [22] R. Buras, H.-T. Janka, M. Rampp, and K. Kifonidis. *Astron. Astrophys.* , **457**, 281, 2006.
- [23] J. W. Murphy and A. Burrows. *Astrophys. J.*, **688**, 1159, 2008.
- [24] A. Marek and H.-T. Janka. *Astrophys. J.*, **694**, 664, 2009.
- [25] C. D. Ott, A. Burrows, L. Dessart, and E. Livne. *Astrophys. J.*, **685**, 1069, 2008.
- [26] C. L. Fryer and M. S. Warren. *Astrophys. J.*, **601**, 391, 2004.
- [27] H.-T. Janka. *Astron. Astrophys.* , **368**, 527, 2001.
- [28] C. L. Fryer and A. Heger. *Astrophys. J.*, **541**, 1033, 2000.
- [29] T. A. Thompson, E. Quataert, and A. Burrows. *Astrophys. J.*, **620**, 861, 2005.
- [30] T. Yamasaki and T. Foglizzo. *Astrophys. J.*, **679**, 607, 2008.
- [31] W. Iwakami, K. Kotake, N. Ohnishi, S. Yamada, and K. Sawada. *submitted to ApJ, arXiv:0811.0651 [astro-ph]*, 2008.
- [32] L. Dessart, A. Burrows, E. Livne, and C. D. Ott. *Astrophys. J.*, **645**, 534, 2006.
- [33] W. Keil, H.-T. Janka, and E. Müller. *Astrophys. J. Lett.*, **473**, L111, 1996.
- [34] A. Marek, H.-T. Janka, and E. Müller. *Astron. Astrophys.* , **496**, 475, 2009.
- [35] K. Kotake, W. Iwakami, N. Ohnishi, and S. Yamada. *Astrophys. J. Lett. in press, arXiv:0904.4300 [astro-ph]*, 2009.
- [36] É. É. Flanagan and S. A. Hughes. *Phys. Rev. D.*, **57**, 4535, 1998.
- [37] R. Adhikari. *Private communication*, 2009.
- [38] URL <http://ligo.caltech.edu>. LIGO.
- [39] R. O'Shaughnessy. *Private communication*, 2009.
- [40] D. Shoemaker. *Private communication*, 2006.
- [41] A. Heger, S. E. Woosley, and H. C. Spruit. *Astrophys. J.*, **626**, 350, 2005.
- [42] C. D. Ott, A. Burrows, T. A. Thompson, E. Livne, and R. Walder. *Astrophys. J. Suppl. Ser.*, **164**, 130, 2006.
- [43] S. E. Woosley and A. Heger. *Astrophys. J.*, **637**, 914, 2006.
- [44] C. L. Fryer and A. Heger. *Astrophys. J.*, **623**, 302, 2005.
- [45] A. Burrows, L. Dessart, E. Livne, C. D. Ott, and J. Murphy. *Astrophys. J.*, **664**, 416, 2007.
- [46] J. M. LeBlanc and J. R. Wilson. *Astrophys. J.*, **161**, 541, 1970.
- [47] D. L. Meier, R. I. Epstein, W. D. Arnett, and D. N. Schramm. *Astrophys. J.*, **204**, 869, 1976.
- [48] G. S. Bisnovaty-Kogan, I. P. Popov, and A. A. Samokhin. *Astrophys. Space Sci.*, **41**, 287, 1976.
- [49] E. M. D. Symbalisky. *Astrophys. J.*, **285**, 729, 1984.
- [50] J. C. Wheeler, D. L. Meier, and J. R. Wilson. *Astrophys. J.*, **568**, 807, 2002.
- [51] S. Akiyama, J. C. Wheeler, D. L. Meier, and I. Lichtenstadt. *Astrophys. J.*, **584**, 954, 2003.
- [52] M. Shibata, Y. T. Liu, S. L. Shapiro, and B. C. Stephens. *Phys. Rev. D.*, **74(10)**, 104026, 2006.
- [53] H. Sawai, K. Kotake, and S. Yamada. *Astrophys. J.*, **672**, 465, 2008.
- [54] T. Takiwaki, K. Kotake, and K. Sato. *Astrophys. J.*, **691**, 1360, 2009.
- [55] S. E. Woosley and J. S. Bloom. *Ann. Rev. Astron. Astrophys.*, **44**, 507, 2006.
- [56] L. Dessart, A. Burrows, E. Livne, and C. D. Ott. *Astrophys. J. Lett.*, **673**, L43, 2008.
- [57] P. Cerdá-Durán, J. A. Font, and H. Dimmelmeier. *Astron. Astrophys.* , **474**, 169, 2007.
- [58] M. Obergaulinger, P. Cerdá-Durán, E. Müller, and M. A. Aloy. *Astron. Astrophys.* , **498**, 241, 2009.
- [59] S. Akiyama and J. C. Wheeler. *Astrophys. J.*, **629**, 414, 2005.
- [60] C. D. Ott, H. Dimmelmeier, A. Marek, H.-T. Janka, I. Hawke, B. Zink, and E. Schnetter. *Phys. Rev. Lett.*, **98**, 261101, 2007.
- [61] C. D. Ott, H. Dimmelmeier, A. Marek, H.-T. Janka, B. Zink, I. Hawke, and E. Schnetter. *Class. Quant. Grav.*, **24**, 139, 2007.
- [62] H. Dimmelmeier, C. D. Ott, H.-T. Janka, A. Marek, and E. Müller. *Phys. Rev. Lett.*, **98(25)**, 251101, 2007.
- [63] H. Dimmelmeier, C. D. Ott, A. Marek, and H.-T. Janka. *Phys. Rev. D.*, **78(6)**, 064056, 2008.
- [64] A. L. Watts, N. Andersson, and D. I. Jones. *Astrophys. J. Lett.*, **618**, L37, 2005.
- [65] J. M. Centrella, K. C. B. New, L. L. Lowe, and J. D. Brown. *Astrophys. J. Lett.*, **550**, L193, 2001.
- [66] C. D. Ott, S. Ou, J. E. Tohline, and A. Burrows. *Astrophys. J.*, **625**, L119, 2005.
- [67] S. Scheidegger, T. Fischer, S. C. Whitehouse, and M. Liebendörfer. *Astron. Astrophys.* , **490**, 231, 2008.
- [68] C. D. Ott, A. Burrows, L. Dessart, and E. Livne. *Phys. Rev. Lett.*, **96(20)**, 201102, 2006.
- [69] N. N. Weinberg and E. Quataert. *Mon. Not. Roy. Astron. Soc.* , **387**, L64, 2008.
- [70] URL <http://www.et-gw.eu>. Einstein Telescope.
- [71] S. Ando, F. Beacom, and H. Yüksel. *Phys. Rev. Lett.*, **95**, 171101, 2005.